

A hierarchical Bayesian model to infer $PL(Z)$ relations using *Gaia* parallaxes

H.E. Delgado¹, L.M. Sarro¹, G. Clementini², T. Muraveva², and A. Garofalo^{2,3}

¹ Dpto. de Inteligencia Artificial, UNED, c/ Juan del Rosal, 16, 28040 Madrid, Spain.

² INAF, Osservatorio di Astrofisica e Scienza dello Spazio di Bologna, via Piero Gobetti 93/3, 40129 Bologna, Italy.

³ Dipartimento di Fisica e Astronomia, Università di Bologna, via Piero Gobetti 93/2, 40129 Bologna, Italy.

Received March 23, 2022; accepted

ABSTRACT

Context. (Gaia Collaboration et al. 2017) analysed exhaustively the Period-Luminosity (PL) and Period-Luminosity(-Metallicity) ($PL(Z)$) relations for Cepheids and RR Lyrae stars using the *Gaia* Data Release 1 (DR1) parallaxes in the Tycho-Gaia Astrometric Solution (TGAS). One of the methods used to infer the relations was based on a hierarchical Bayesian model, the description of which was deferred to a subsequent publication that is presented here.

Aims. We aim at creating a Bayesian model to infer the coefficients of PL or $PL(Z)$ relations that propagates uncertainties in the observables in a rigorous and well founded way.

Methods. We propose a directed acyclic graph to encode the conditional probabilities of the inference model that will allow us to infer probability distributions for the PL and $PL(Z)$ relations. We evaluate the model with several semi-synthetic data sets and apply it to a sample of 200 fundamental mode and first overtone mode RR Lyrae stars for which *Gaia* DR1 parallaxes and literature K_s -band mean magnitudes are available. We define and test several hyperprior probabilities to verify their adequacy and check the sensitivity of the solution with respect to the prior choice.

Results. We find that our Bayesian model successfully infers probability distributions for the RR Lyrae PLZ relation in the K_s -band when it is applied to semi-synthetic data. We find that our model systematically underestimates the slope corresponding to the period term of the PLZ relation when it is applied to the *Gaia* DR1 RR Lyrae sample. We demonstrate that this underestimation is due to the correlation between periods and TGAS parallaxes, which in turn is a consequence of the fact that period and metallicity are correlated in RR Lyrae stars (with shorter periods being characteristic of higher metallicities).

Key words. methods: data analysis – methods: statistical – stars: variables: RR Lyrae – parallaxes

1. Introduction

Cepheids and RR Lyrae stars are primary standard candles of the cosmological distance ladder because they follow canonical relations that for Cepheids link the star intrinsic luminosity (L) to the period (P) of light variation (traditionally referred to as period-luminosity (PL) relation or Leavitt Law), whereas for RR Lyrae stars link L in the infrared passbands to P and possibly the stellar metallicity (Z ; PL - metallicity relation – $PL(Z)$) or L in the visual passband to Z (traditionally referred to as RR Lyrae luminosity - metallicity relation). The predicted precision of the *Gaia* end-of-mission parallaxes for local Cepheids and RR Lyrae stars¹ will allow us to determine the slope and zero point of these fundamental relations with unprecedented accuracy, thus setting the basis for a global reassessment of the whole cosmic distance ladder. As a first anticipation of the *Gaia* potential in this field of the cosmic distance ladder and a first assessment of improved precision with respect to previous astrometric missions such as, for instance, Hipparcos, and the dramatic increase in statistics compared to what is achievable for instance, measuring parallaxes with the Hubble Space Telescope, *Gaia* DR1 published parallaxes for more than 700 Galactic Cepheids and RR Lyrae stars, computed as part of the Tycho-*Gaia* Astrometric Solution (TGAS; (Lindgren et al. 2016)). In (Gaia Collaboration et al.

2017, hereafter Paper I) we have used TGAS parallaxes, along with literature photometry and spectroscopy, to calibrate the zero point of the PL relations of classical and type II Cepheids, and the near-infrared PL and $PL(Z)$ relations of RR Lyrae stars by fitting these relations adopting different techniques that operate either in parallax or distance (absolute magnitude) space. In that paper different sources of biases affecting the TGAS samples of Cepheids and RR Lyrae stars were discussed at some length and the possible systematic errors caused in the inferred luminosity calibrations were analysed in detail.

Section 3.2 of Paper I in particular discussed the problem of fitting general luminosity relations between the absolute magnitude M_{True} , the decadic logarithm of the period P_{True} and possibly also the metallicity $[\text{Fe}/\text{H}]_{\text{True}}$ of the form

$$M_{\text{True}} = b + c \cdot \log(P_{\text{True}}) + k \cdot [\text{Fe}/\text{H}]_{\text{True}} \quad (1)$$

with a sample that is truncated in parallax (by removing the non-positive values) and for which the assumption of normality of uncertainties in the absolute magnitude is not valid. These problem arise if we directly estimate absolute magnitudes using

$$M = m + 5 \log(\varpi) - 10, \quad (2)$$

where m is the measured apparent magnitude and ϖ is the measured parallax. First, if parallaxes are negative, then absolute

¹ See <https://www.cosmos.esa.int/web/gaia/science-performance>

magnitudes can not be computed at all, causing a problem of sample representativeness due to the selective removal of distant sources. Second, even for positive parallaxes with uncertainties approximately normally distributed, the logarithmic term in Eq. 2 induces non-Gaussian uncertainties in absolute magnitudes, discouraging the application of the ordinary least squares (OLS) method to fit the model prescribed by Eq. 1. Each of these problems leads to potential biases in the inference of the slopes and zero point of Eq. 1.

In order to circumvent these difficulties one first has to bear in mind that Eq. 2 is only valid for the true values of the absolute and apparent magnitudes and the parallax. We never have access to the true parallax and thus, we are forced to use estimates. While the measured parallax ϖ is an unbiased estimator of ϖ_{True} when the measurement uncertainties are Gaussian, the quantity $m + 5 \log(\varpi) - 10$ is not a good estimator of the true absolute magnitude due to the decadic logarithm in Eq. 2. Also, measured parallaxes may be negative or zero but true parallaxes are always positive. If we remove the non-positive measurements we are truncating the sample by removing the furthest and faintest objects, thus biasing again the results (see Luri et al. 2018, for a more detailed description of the intricacies involved in using astrometric measurement for the inference of quantities of astrophysical interest). Our proposal in Paper I was to construct a two-level statistical model that distinguishes between true and measured parallaxes. This model can then be used to infer the true parallaxes from the measurements and apply Eq. 2 to infer true absolute magnitudes. The natural way to construct such a model is to apply the Bayesian methodology where one assigns a prior probability distribution to the true parallax population. In doing so, a suitable selection of this prior will improve the estimation of individual true parallaxes in the sense that their posterior credible intervals are 'shrunk' with respect to the measurement uncertainties. Setting a specific prior is always controversial, but in principle it is possible to define only a functional form that depends on a set of unknown parameters. The specific prior is then inferred from the data as part of the global inference process. This prior functional form should be flexible enough to properly model the true distribution of parallaxes but also should be sufficiently restrictive to enforce a plausible distribution for the true parallaxes on the basis of the knowledge present in the astronomical literature.

The solution described in the previous paragraph can be represented as a graph model that simultaneously includes the relationships of Eqs. 1 and 2, their astrophysical parameters (of which m and ϖ represent now the true apparent magnitude and the true parallax) and the corresponding measurements and uncertainties. This way we guarantee that the observational uncertainties are simultaneously propagated through the graph and that the uncertainties of the parameters of the *PLZ* relationship are estimated in a way that is consistent with the measurement uncertainties. Also, the effect of including the relationship

$$b + c \cdot \log P + k \cdot [\text{Fe}/\text{H}] = m + 5 \log \varpi - 10 \quad (3)$$

in the model is to constrain the parameter space in such a way that the *PLZ* relationship coefficients and the individual true parallaxes have to be consistent.

The objective of this paper is to infer estimates of the parameters of the *PLZ* relationship. We apply the hierarchical Bayesian methodology, which consists in dividing the variability of the statistical inference problem into several levels. In this way we partition the parameter space associated to inferring the *PLZ* relation into population-level parameters and observations. We

represent the hierarchical Bayesian model with a directed acyclic graph and perform the inference using Markov chain Monte Carlo (MCMC) simulation techniques (Robert & Casella 2013). A minimal description of the methodology and preliminary results was already presented in Paper I which we intend to extend and clarify here. For reasons of clarity and scope we focus on the inference of the *PLZ* relationship in the *K*-band for 200 fundamental and first overtone RR Lyrae stars, the main properties of which are provided in Table A.3 of Paper I. The model is applicable with minimal modifications to other variability types such as Cepheids or Long Period Variables and different photometric bands. In this work we present the results of the full model including the slopes of the relation, expanding the results presented in Paper I where only the zero points were inferred while the slopes were fixed to literature values.

A similar methodology has been applied by Sesar et al. (2017) to constrain *PLZ* relations of RR Lyrae stars in the mid-infrared W1 and W2 bands on the Wide-field Infrared Survey Explore (WISE; Wright et al. (2010)), using TGAS parallaxes, but modelling true distances with an exponentially decreasing volume density (hereafter EDVD) prior proposed by Bailer-Jones (2015).

In Paper I, given the large uncertainties of the TGAS parallaxes, the authors were forced to fix the slope of the $\log(P)$ term of the *PLZ* relation to literature values and only infer the zero point by three different methods. In particular, the Bayesian hierarchical method used a log-normal prior to model the distribution of true parallaxes. With this prior, the $\log(P)$ slope turned out to be severely underestimated when compared to the literature values, although this result was not specifically discussed therein. In the present work we extend the Bayesian analysis performed on Paper I in three directions. First, we validate the model with semi-synthetic data and analyse the causes of the slope underestimation. We demonstrate that such an underestimation is mainly caused by a correlation between period and parallax, that we hypothesize is due to the correlation between periods and metallicities of RR Lyrae stars, and metallicities and distances of the RR Lyrae stars in the present sample. This results in a sample that is biased towards higher luminosities at greater distances and *viceversa*. Second, we extend the Bayesian analysis by using two alternative prior distributions for parallaxes and demonstrate that one of them mitigates to some degree the problem of the underestimation of the *PLZ* $\log(P)$ slope. Third, we study the sensitivity of the Bayesian analysis results under different prior choices for some critical hyperparameters of our hierarchical model (HM).

The structure of the paper is as follows. In Sect. 2 we summarize the theoretical foundations of the hierarchical Bayesian methodology and describe extensively the HM used for inferring the *PLZ* relationship proposed in Paper I. In Sect. 3 we evaluate the model and explore its boundaries and limitations; in Sect. 4 we present the full results of the MCMC samples of the posterior distribution for the Gaia DR1 data used in Paper I; in Sect.5 we describe the three alternative prior distributions used in our HM and study their impact on the inferred posterior distributions of the parameters of the *PLZ* relationship; in Sect. 6 we study the sensitivity of the results to the choice of hyper-parameters, and in Sect. 7 we summarise the findings of this analysis.

2. The hierarchical Bayesian model description

2.1. Hierarchical modelling

A full introduction to Bayesian inference and hierarchical Bayes is beyond the scope of this manuscript. We recommend the interested reader to consult Gelman et al. (2004) and Gelman & Hill (2007) for very pedagogic introductions, and Luri et al. (2018) for a more Astronomy-oriented introduction. In what follows, we summarize the main concepts of the methodology. Bayesian inference is based on Bayes' rule:

$$p(\Theta | \mathcal{D}) \propto p(\mathcal{D} | \Theta) \times p(\Theta), \quad (4)$$

where \mathcal{D} are the observations (data), Θ are the parameters of a model proposed to explain the data and p represents a probability distribution. The right side of Eq. 4 represents the model itself, specified by the joint probability distribution $p(\mathcal{D}, \Theta)$ of the data and the parameters. This distribution factorizes into:

- the conditional distribution $p(\mathcal{D} | \Theta)$ of the data given the parameters (the so called *likelihood*), and
- the *prior* distribution of the parameters $p(\Theta)$, which represents our knowledge about plausible parameter values before observing the data.

The basic model of Eq. 4 divides the variability of the statistical problem into two levels: observations and parameters. The hierarchical Bayesian methodology consists in distinguishing further levels of variability. In our case, we introduce a new dependence of the prior distribution $p(\Theta)$ on a new set of parameters Φ (the so called *hyperparameters*) and assign *hyper-prior* distributions $p(\Phi)$ to them. We explain its nature in the following Sections. In order to have a better understanding of the dependency structure dictated by the model, it is customary to represent the factorization of the joint probability distribution $p(\mathcal{D}, \Theta, \Phi)$ by using the Bayesian network formalism (Pearl 1988; Lauritzen 1996), which consists in drawing a DAG (directed acyclic graph) in which nodes encode model parameters, measurements or constants, and directed links represent conditional probability dependence relationships.

The inference in a hierarchical Bayesian model proceeds by calculating the *marginal joint posterior* distribution of a set of *parameters of interest* given the data. The task, although analytically intractable in complex situations with many parameters, is nowadays straightforward by sampling from the posterior distribution using MCMC simulation technics.

2.2. Observations, true parameters and the $PL(Z)$ relationship

In this and the next Section we describe the hierarchical model that encodes the conditional probability relations between the observations and the parameters of the linear $PL(Z)$ relations. We include Fig. 19 of Paper I here as Fig. 1, to facilitate reading, but include some additional clarifications that could not be described there due to space and scope limitations.

In the following, we will change the notation to avoid cluttering of subscripts. Henceforth, we will denote measured quantities with a circumflex accent ($\hat{}$) and remove the subscript True from the true values. The DAG in Figure 1 encodes the probabilistic relationships between the variables of our model and shows the measurements at the bottom level: decadic logarithm of periods $\log \hat{P}_i$, apparent magnitudes \hat{m}_i , metallicities $[\widehat{\text{Fe}/\text{H}}]_i$,

parallaxes $\hat{\varpi}_i$ and extinctions \hat{A}_{m_i} . The subindex i runs from 1 to the total number of stars N in each sample. Our model assumes that the measurements

$$\mathbf{d}_i = (\hat{m}_i, \log \hat{P}_i, \hat{\varpi}_i, [\widehat{\text{Fe}/\text{H}}]_i, \hat{A}_{m_i}), \quad (5)$$

are realizations from normal distributions centred at the true (unknown) values and with standard deviations given by the measurement uncertainties. In Paper I we used the literature uncertainties for the apparent magnitudes and metallicities, and TGAS uncertainties for the parallaxes (Lindegren et al. 2016). The uncertainties for the periods of these well studied stars were not available, but we consider them small enough to approximate them with a standard deviation of 0.01 dex where the periods are measured in days. All measured quantities are represented as blue nodes in the DAG.

We represent the likelihood of the model with the nodes corresponding to the true values $m_i, \varpi_i, \log P_i, [\text{Fe}/\text{H}]_i$ and A_{m_i} and the arcs going from true values to measurements. Note that true values and observations are all enclosed in a black rectangle that represents replication for the N stars in the sample (plate notation). Equation 1 can be written for every star i in the sample as

$$M_i = b + c \cdot \log P_i + k \cdot [\text{Fe}/\text{H}]_i, \quad (6)$$

where M_i represents the true absolute magnitude for star i . This is a linear model in the parameters: the intercept b , the slope c for the period term, and the slope k for the metallicity term. The last term can be dropped if metallicities are thought to play a negligible role in the relationship. We keep it in the following for the sake of completeness, but the particularization to PL relations is straightforward. In Fig. 1 we shadow the left hand rectangle that includes the metallicity terms to remark this choice. In practice, it is more convenient to recast Eq. 6 as

$$M_i = b + \tan(\phi_1) \cdot \log P_i + \tan(\phi_2) \cdot [\text{Fe}/\text{H}]_i, \quad (7)$$

where $c = \tan(\phi_1)$ and $k = \tan(\phi_2)$, for reasons that we will explain later. In Fig. 1, the $PL(Z)$ relationship of Eq. 7 is denoted by the grey node M_i and all incoming arrows from ϕ_1, ϕ_2, b, P_i and $[\text{Fe}/\text{H}]_i$ (that is, the three parameters and two predictive variables). In fact, the reader may have noticed that there is an additional arrow linking w and M_i . w represents an intrinsic width in the $PL(Z)$ relationship that may be due to evolutionary effects, for example. This dependence on additional predictive variables that are not accounted for in the model is incorporated as an additional Gaussian spread of standard deviation w . This additional spread will be analysed as part of the inference results. Including the additional Gaussian spread that represents unaccounted predictive variables, we have that

$$M_i \sim \text{N}(b + \tan(\phi_1) \cdot \log P_i + \tan(\phi_2) \cdot [\text{Fe}/\text{H}]_i, w), \quad (8)$$

where \sim should be read as 'is distributed as', N represents the normal (Gaussian) distribution, and the comma separates values inside the parenthesis that represent the mean and standard deviation of the normal distribution, respectively.

Of course, we do not observe absolute magnitudes, and our model has to account for the transformation between absolute magnitudes and the observations, that are (potentially affected by interstellar absorption) apparent magnitudes. This is shown in

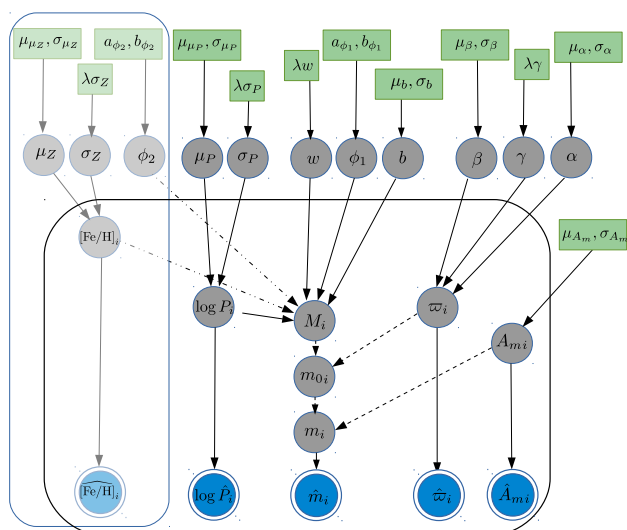


Fig. 1: Directed Acyclic Graph that represents the forward model used to infer the PLZ relation coefficients when the prior of true parallaxes is assumed to be a log-skew-normal distribution.

the lower part of Fig. 1, where the parallaxes (right-hand block) are handled as we explain next.

The transformation from absolute to apparent magnitudes is a well known deterministic one:

$$m_{0i} = M_i - 5 \log(\varpi_i) + 10, \quad (9)$$

where the parallax ϖ_i is measured in mas. This is not a probabilistic relation and we use dashed lines in the arrows going into m_{0i} to distinguish them from the arcs denoting conditional probability links. The apparent magnitudes are computed as $m_i = m_{0i} + A_{m_i}$, where the gray node A_{m_i} represents the true absorption.

2.3. Priors, hyperparameters and hyperpriors

Prior distributions allow us to pose probabilistic statements about plausible values of the model parameters based on knowledge available prior to and independent of the observations. But most important, they allow us by means of Bayes' theorem to make statements about the distribution of the parameters we aim to infer (the posterior distribution of the model parameters in the left side of Equation 4). In the astrophysical context of this paper, we aim at formulating probabilistic statements about the values of the hyperparameters: the most probable value of the $PL(Z)$ slopes or intercepts or their credible intervals. We use green rectangular nodes at the top of the graph to denote fixed prior hyperparameters.

Often the prior definitions used in the literature are conservative choices in the sense that they aim to be as non-informative as possible. For the angles ϕ_1 and ϕ_2 of the $PL(Z)$ relationship of Eq. 7 we specify uniform priors supported on the intervals $[a_{\phi_1} = -\pi, b_{\phi_1} = 0]$ and $[a_{\phi_2} = -\pi/6, b_{\phi_2} = \pi/6]$. Note that this is much easier than directly assigning non-informative priors to the slopes $c = \tan(\phi_1)$ and $k = \tan(\phi_2)$. Slopes have infinite support (that is, they can take values between $-\infty$ and ∞) and assigning them uniform priors will inevitably give more probability weight to larger slopes due to the non-linear relationships

between angles and slopes. A uniform prior for the slope is therefore a very informative one. The prior probability distribution of the intercept is a Gaussian centred at $\mu_b = 0$ with $\sigma_b = 10$. The intrinsic scatter of the PLZ relation is given an exponential prior with inverse scale $\lambda_w = 1$.

The true values of $\log P_i$ and $[Fe/H]_i$ are modelled as realizations from Gaussian distributions. These priors have the location hyperparameters μ_P and μ_Z and the scale hyperparameters σ_P and σ_Z . We assign non-informative Gaussian hyperpriors with mean 0 and standard deviation 10 for the central hyperparameters and exponential hyperpriors with inverse scale equal to 0.1 for the scale hyperparameters.

The only block of the graph that remains to be clarified is the one describing the distribution of parallaxes. It is in this block that the full power of hierarchical models becomes more evident. We circumvent the problem of prior choice by defining one, whose parameters are also part of the model parameters. This is what we represent in the parallax block of the graph. We define a log-skew-normal prior for the parallaxes ϖ_i

$$\varpi_i \sim \text{logSN}(\beta, \gamma, \alpha), \quad (10)$$

where the hyperparameters β , γ and α are respectively the location, scale and shape of the skew-normal distribution (Azzalini 1985) that describes $\ln \varpi$. The location, scale and shape are themselves model parameters and subject of the Bayesian inference as well. As such, they have their own hyperpriors: a normal distribution with mean $\mu_\beta = 0$ and standard deviation $\sigma_\beta = 10$ for β , an exponential distribution with inverse scale parameter $\lambda_\gamma = 0.01$ for γ , and a half-normal distribution with mean $\mu_\alpha = 0$ and standard deviation $\sigma_\alpha = 10$ for α . The normal prior for $\ln \varpi$ used in Paper I is a particular case of the skew-normal when the skewness parameter $\alpha = 0$. Hence, our new prior for the parallaxes is as flexible as the prior hyperparameters allow and more flexible than the original one.

Fig. 2 includes the parallaxes from TGAS used in Paper I and a random sample of ten logskewed normal parallax priors from the hyperpriors prescriptions, showing a reasonable flexibility. The ten priors have been normalized in height for clarity. The blue histogram corresponds to the TGAS measured parallaxes for the sample of 200 RR Lyrae stars used in Paper I. We draw the attention to the negative parallaxes measured in TGAS, and the need for an extended wing in the prior probability that accounts for the parallaxes beyond 2 mas. The prior distribution is meant to describe the distribution of true (not measured) parallaxes and therefore can only be non-zero for positive values.

Fig. 1 translates into the following likelihood

$$p(\mathcal{D} | \Theta) = \prod_{i=1}^N p(\mathbf{d}_i | \Theta) = \prod_{i=1}^N p\left([\widehat{Fe/H}]_i | [Fe/H]_i, \sigma_{Z_i}\right) \cdot p\left(\log \hat{P}_i | \log P_i, \sigma_{P_i}\right) \cdot p\left(\hat{m}_i | M_i, A_{m_i}, \varpi_i, \sigma_{m_i}\right) \cdot p\left(\hat{\varpi}_i | \varpi_i, \sigma_{\varpi_i}\right) \cdot p\left(\hat{A}_{m_i} | A_{m_i}\right) \quad (11)$$

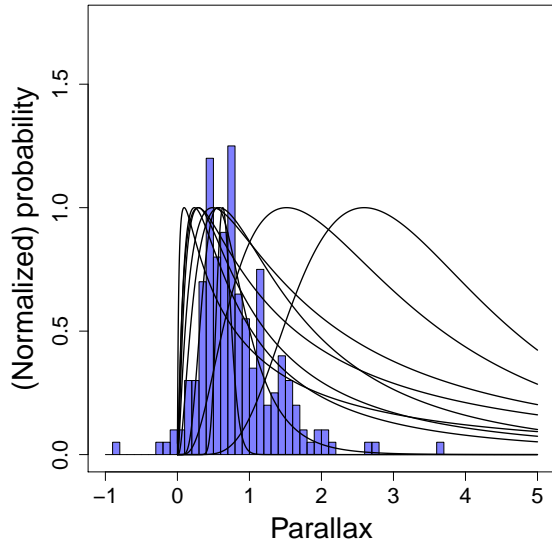


Fig. 2: Histograms of TGAS parallaxes for the RR Lyrae stars sample used in Paper I. The blue histogram corresponds to the sample of RR Lyrae stars. The solid lines correspond to a sample of ten random priors drawn from the hyperprior.

and priors:

$$\begin{aligned}
\pi(\Theta) = & \pi(\mu_Z, \sigma_P) \cdot \pi(\mu_P, \sigma_P) \cdot \pi(b, \phi_1, \phi_2, w) \cdot \pi(\beta, \gamma, \alpha) \\
& \cdot \prod_{i=1}^N \pi([\text{Fe}/\text{H}]_i | \mu_Z, \sigma_Z) \cdot \pi(\log P_i | \mu_P, \sigma_P) \\
& \cdot \pi(M_i | b, \phi_1, \phi_2, w, \log P_i, [\text{Fe}/\text{H}]_i) \\
& \cdot \pi(\varpi_i | \beta, \gamma, \alpha) \cdot \pi(A_{m_i})
\end{aligned} \tag{12}$$

where each prior probability is defined in Table 1.

We have encoded our HM using the Stan probabilistic modelling language (Carpenter et al. 2017) and used the No-U-Turn sampler (NUTS) of Hoffman & Gelman (2014) to compute the MCMC samples corresponding to the parameters of interests.

$$\begin{aligned}
\pi(M_i | b, \phi_1, \phi_2, w, \log(P_i), [\text{Fe}/\text{H}]_i) &= \text{N}(b + \tan(\phi_1) \cdot \log(P_i) + \tan(\phi_2) \cdot [\text{Fe}/\text{H}]_i, w) \\
\pi(\log(P_i) | \mu_P, \sigma_P) &= \text{N}(\mu_P, \sigma_P) \\
\pi([\text{Fe}/\text{H}]_i | \mu_Z, \sigma_Z) &= \text{N}(\mu_Z, \sigma_Z) \\
\pi(\varpi_i | \beta, \gamma, \alpha) &= \log\text{SN}(\beta, \gamma, \alpha) \\
\pi(b) &= \text{N}(0, 3) \\
\pi(\phi_1) &= \text{U}(-3.14/2, 0) \\
\pi(\phi_2) &= \text{U}(-3.14/6, 3.14/6) \\
\pi(w) &= \text{Exp}(1) \\
\pi(\mu_P) &= \text{N}(0, 10) \\
\pi(\sigma_P) &= \text{Exp}(0.1) \\
\pi(\mu_Z) &= \text{N}(0, 10) \\
\pi(\sigma_Z) &= \text{Exp}(0.1) \\
\pi(\beta) &= \text{N}(0, 10) \\
\pi(\gamma) &= \text{Exp}(0.05) \\
\pi(\alpha) &= \text{HN}(0, 10) \\
\pi(\gamma) &= \text{Exp}(0.05)
\end{aligned}$$

Table 1: Prior (π) definitions for the hierarchical Bayesian model of the $PL(Z)$ relations. We use the π symbol to refer to the prior probability and use 3.14 to refer to the half-length of the unit circumference.

3. Model validation

In Paper I, due to the high uncertainties on the TGAS parallaxes, only the zero point of the PLZ relation was inferred while the slopes were fixed to literature values. In what follows we eliminate this restriction and evaluate the accuracy of our HM to infer the coefficients of the PLZ relationship under two simulated scenarios that only differ on the measured parallaxes and their uncertainties. In both scenarios we assume that there is a certain and fixed PLZ relationship of the form given by Eq. 8, that dictates the dependency of the absolute magnitudes on the periods and metallicities of our sample.

In this Section, we aim at validating the model on synthetic data as close as possible to the true data set but following exactly a PLZ relation from the literature. We simulate a set of semi-synthetic true absolute magnitudes and parallaxes using the PLZ relation and the apparent magnitudes of the sample used in Paper I. Our objective is to analyse the impact of the hyperprior choice, the influence of the parallax uncertainties on the inferred coefficients under the two scenarios and detect potential biases in the sample. In what follows, we describe the construction of the two data sets A and B that reproduce the generative process of the observations of Eq. 5 from the model hyper-parameters for both scenarios. The only difference between the two synthetic data sets lies in the assumed parallax uncertainties. In data set A we generate parallax uncertainties from an hypothesized distribution, and in data set B we use the TGAS uncertainties.

In the generation of the semi-synthetic samples we first infer the distribution of true periods and metallicities from the measured values in the data set used in Paper I. We use a Bayesian model where the true logarithms of the period and the metallicities are assumed to be Gaussian-distributed, and the observed values are drawn from a Gaussian distribution centred at the true value and with standard deviation given by the measurement uncertainties. Then, for both data sets we have drawn true logarithms of the period and metallicities from the posterior distributions given their measurements in the real (non-simulated) RR Lyrae sample. We have generated true absolute magnitudes and true parallaxes respectively from Equation 4 of Muraveva et al. (2015)

$$M_{K_s} = -2.73 \log P + 0.03 [\text{Fe}/\text{H}] - 1.06 \quad (13)$$

and from

$$\varpi_i = 10^{2+0.2(M_i-m_{0i})}, \quad (14)$$

where m_{0i} is the dereddened apparent magnitude of the i -th star in the real sample. For data set A we have generated measured parallaxes from a Gaussian distribution centred at the true parallaxes given by Eq. 14 and with standard deviations drawn from an exponential distribution with inverse scale parameter equal to 10 plus a zero-point of 0.01 mas. Note that the uncertainties on TGAS parallaxes are higher than these ones by approximately one order of magnitude, but our objective here is to evaluate the performance of our HM under moderately low, but plausible, parallax uncertainties. The measured parallaxes of data set B were generated using the TGAS parallax uncertainties.

Figure 3 represents in the top panel the values of the absolute magnitude and logarithm of the period generated for simulation B. The red line shows the PL relation for the median value of $[\text{Fe}/\text{H}]$ in the simulated sample. Since this plot is a 2D projection of the 3D PLZ relation, and the absolute magnitudes were calculated exactly from it, any deviations from the red line are simply due to metallicities different from the median. The colour code reflects the values of the observed parallax. A correlation between periods and metallicities is evident which results in correlated residuals (lower panel) with respect to the assumed PL for the median metallicity. This correlation is not an added effect in the simulations. It is already present in the data set used in Paper I as shown in Figure 4.

Fig. 5 compares the true periods and parallaxes (the same for simulations A and B). The colour code reflects the metallicity as shown in the colour scale on the right hand side of the plot. In principle, one expects the distribution of periods to be independent of distance. However, Figure 5 shows a slight decrease of the median period calculated in bins of parallax as the parallax value increases. A similar systematic correlation affects metallicities, with median metallicities increasing as the parallax increases. We interpret the former as the result of the latter, together with a non-uniform distribution of metallicities in the spatial volume probed by our sample. The interpretation is as follows: we expect nearby stars in our sample to be characterised on average by the higher metallicities of the disk, while the opposite is true for those further away in the halo. This distance-metallicity relation is visible in the colour code of Figure 5.

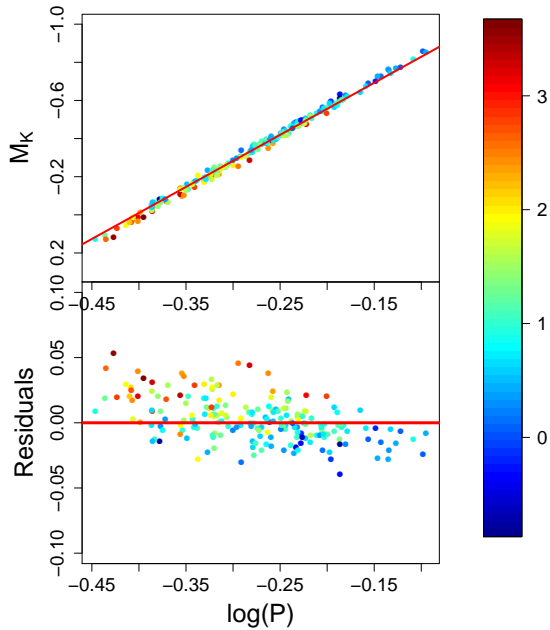


Fig. 3: Plot of the observed absolute magnitudes as a function of the observed decadic logarithm of the period for simulation B (parallax uncertainties taken from TGAS). The red solid line represents the PLZ relation by Muraveva et al. (2015) for the K -band and a value of the metallicity equal to the median of the values generated according to the text. Colours encode the simulated observed parallaxes according to the scale on the right.

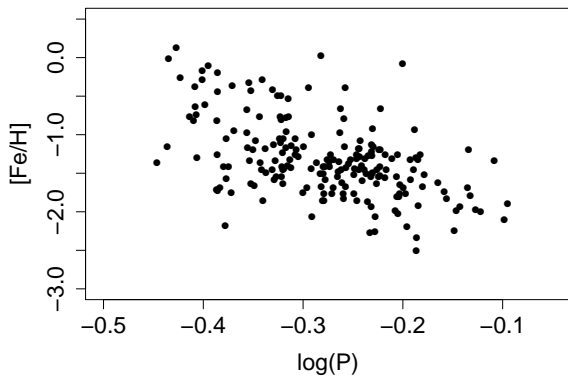


Fig. 4: Scatter plot of metallicities and $\log(P)$ for the sample used in Paper I.

Since higher metallicities correspond to shorter periods (as illustrated in Figure 4) we then expect the nearby stars (that let us recall, are on average more metallic) to be characterised by shorter periods (the left half of the period luminosity diagram). And the opposite is also true: the distant (small parallax) halo stars have on average lower metallicities and hence, larger parallaxes (the right half of the PL diagram). This scenario is then prone to systematic biases in the $\log(P)$ slope inference results because it is precisely at the right edge of the PL diagram that there is a concentration of the most distant sources that will inevitably

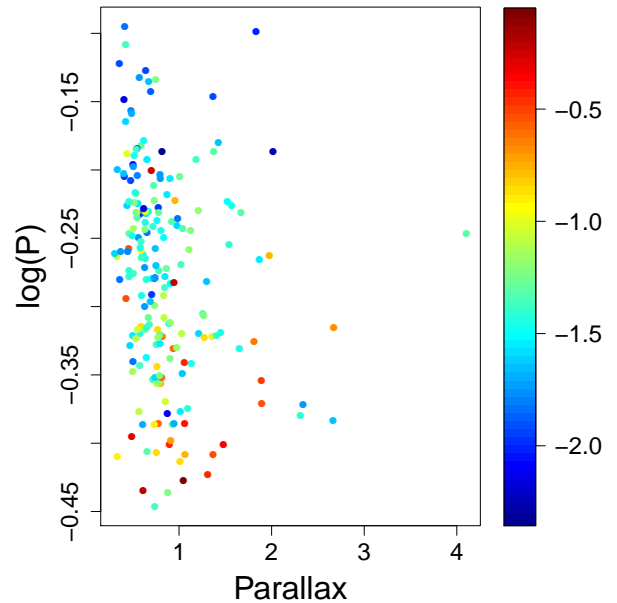


Fig. 5: Comparison between simulated true parallaxes and periods of validation sets A and B. Colours represent simulated metallicities.

be characterised by larger fractional parallax uncertainties. We know that in general, the prior plays a minor role whenever the uncertainties are small because a narrow likelihood dominates the posterior. And the opposite is true for stars with large fractional parallax uncertainties: the likelihood is barely informative and it is the prior that dominates the posterior. Bailer-Jones (2015) shows very pedagogic illustrations of this for the problem of inferring distances for parallaxes under several prior specifications. In our case, the stars for which the prior has a larger impact on the inference of the parallax are predominantly placed at the rightmost range of periods.

These relatively hidden correlations will have important consequences for the inference as we will see. In particular, it will have an impact on the choice of prior. In general, the parallax prior has to have support (non-vanishing values) in all the range of true parallaxes. But this is even more important given the correlation between periods and true parallaxes because in the case of our simulations, long periods have on average the smallest parallaxes. If the prior has zero probability density for the small true parallaxes, and given the relatively large parallax uncertainties in our sample, the model will systematically assign parallaxes larger than the true ones (will overestimate them) and hence for the same apparent magnitude, will infer absolute magnitudes fainter than the true ones. Finally, if the long period variables get fainter absolute magnitudes, the model will systematically underestimate the period slope coefficient of the PLZ relation. The problem is that, if our interpretation is correct, the distance prior should depend on metallicity.

Without a proper modelling of the selection effect that gives rise to this correlation between periods and true parallaxes, the inference will return a severely underestimated $\log(P)$ slope. Fig. 6 illustrates the effect of this underestimation. It compares the parallaxes inferred by the HM with the true ones simulated for datasets A (top panel) and B (bottom panel). The colours in both

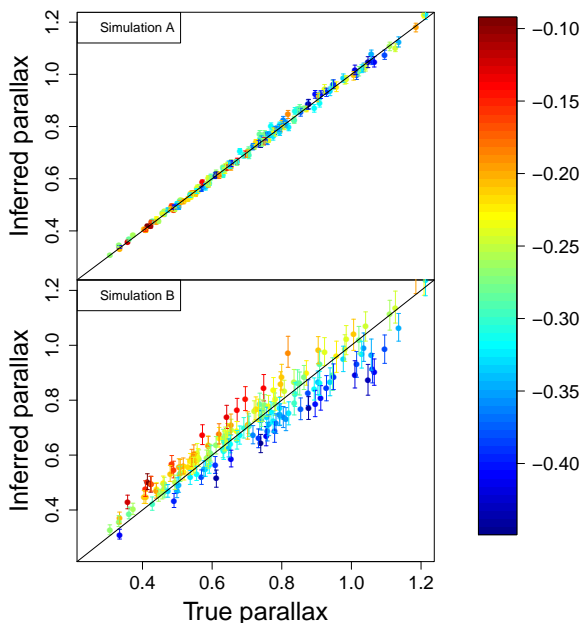


Fig. 6: Comparison between inferred and true parallaxes for validation sets A and B. The colour encodes the value of the decadic logarithm of the period in days according to the colour scale on the right.

panels represent the $\log(P)$ according to the colour scale to the right. For simulation B we observe that lower parallaxes (typical of the longer periods) are systematically overestimated and *viceversa*. We also observe that lower and overestimated parallaxes ($\varpi_{\text{True}} \lesssim 0.6$) correlate with higher periods; higher and underestimated parallaxes ($\varpi_{\text{True}} \gtrsim 0.8$) correlate with lower periods.

Given that in both simulated data sets, the full range of absolute magnitudes is reduced to the lower and higher magnitude ranges for lower and higher parallaxes respectively, and because the strong deterministic relationship between absolute magnitudes and true parallaxes established by Eq. 9 of the HM, in the inference we obtain overestimated lower absolute magnitudes associated to underestimated lower parallaxes and *viceversa*. Fig. 7 illustrates this bias by comparing the inferred absolute magnitudes for simulations A and B to the true periods used in both simulations. We observe in the bottom panel of the Figure that lower luminosities are overestimated for short period stars and *viceversa*. The impact of the bias is greatly reduced in the data set A (upper panel) because the negligible parallax uncertainties tightly constrain the model parameters (the true parallaxes and hence, the absolute magnitudes and the slopes of the relation). In fact, the posterior median of the $\log(P)$ slope inferred by the HM for simulation A was ≈ -2.76 mag/dex, which is in good agreement with the value of -2.73 used for the simulation. On the contrary, for data set B (lower panel) the large TGAS uncertainties associated to the observed parallaxes result in a severe underestimation of the relation slope (in this case we obtained a posterior median ≈ -0.87 mag/dex). Even if the effect on the model slopes and inferred true parallaxes in data set A is small, the correlation between parallaxes and periods is still clearly visible in the top panel of Fig. 6.

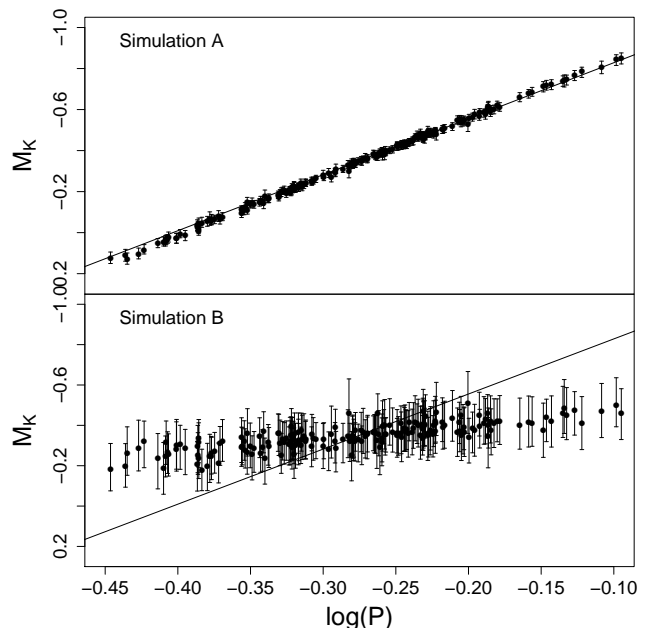


Fig. 7: Comparison between inferred absolute magnitudes and true periods for validation sets A and B. The solid line represents the PLZ relation by Muraveva et al. (2015) for the K -band and a value of the metallicity equal to the median of the values generated according to the text.

4. Application to the RR Lyrae Gaia DR1 data

Fig. 8 shows the MCMC posterior samples (in 2D projections) of the PLZ relationship parameters obtained by our HM when it is trained with the sample of RR Lyrae used in Paper I. The red contours represent iso-probability lines. We see clear correlations between the three strong parameters (intercept and the two angles). The correlation is non-linear in the $\log(P)$ angle and results in a clearly asymmetric marginal posterior probability distribution as shown in the bottom right histogram. The posterior medians of the $\log(P)$ angle, the metallicity angle and the intercept are, respectively, ≈ -0.70 rad, $\approx +0.07$ rad and ≈ -0.60 mag. The posterior medians of the transformed parameters $\tan(\phi_1)$ and $\tan(\phi_2)$ that correspond to the slopes of the $\log(P)$ and metallicity terms of the PLZ relationship are ≈ -0.85 and $\approx +0.08$ mag/dex. This values are in bad agreement with those reported in the literature (see Table 3 of Muraveva et al. (2015)). In particular, the $\log(P)$ slope (in absolute value) seems to be severely underestimated by the HM and the zero-point is systematically higher than the reported values by more than $\approx +0.5$ mag. The posterior median of the intrinsic width is ≈ 0.18 mag.

Fig. 9 shows a comparison between the parallaxes catalogued in TGAS and the maximum a posteriori estimates of our hierarchical model. The horizontal error bars represent TGAS uncertainties and the vertical ones represent the standard deviation of the marginal posterior. We use the standard deviation because the posterior samples for individual star parallaxes remain Gaussian and therefore symmetric. We see that our hierarchical model is capable of reducing (“shrinking”) the uncertainties using the constraint that the absolute magnitudes must follow a linear relationship with (the logarithm of the) periods and metallicities, albeit with a slope in disagreement with previous estimates. The mode of the standard deviations of the posterior samples is

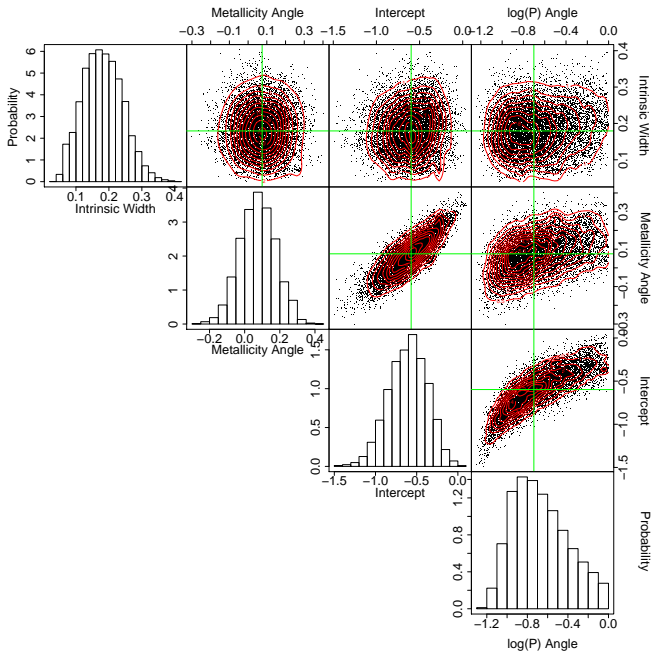


Fig. 8: Marginal posterior distributions from the MCMC samples of the PLZ relationship parameters for the HM with a log-skew-normal prior for parallaxes. The diagonal shows the unidimensional marginal distributions for the intrinsic width of the relationship, the angle of the metallicity term in the linear relation, the intercept and the angle of the $\log(P)$ term.

0.05 mas with a maximum value of 0.2, which is the minimum value of the TGAS parallaxes uncertainties. As shown in Fig. 9, the maximum standard deviation of the MCMC parallax samples corresponds to the same stars with minimum TGAS uncertainties (those with maximum TGAS parallax measurements). This means that the hierarchical model is not capable of significantly improving the parallax uncertainties of the stars near the Sun. We also see that there are stars with TGAS and HM parallaxes that disagree beyond the error bars. We plot in red the stars with Mahalanobis distances from the diagonal between 2 and 3.

Fig. 10 shows the PL relations derived from the HM. Each grey line corresponds to one sample in the Markov chain. All PLZ relations have been particularized to a value of the metallicity $[\text{Fe}/\text{H}] = -1.46$ dex, which is the mode of the distribution of measured values. On the left hand panel we show the values of the absolute magnitude in the K band derived from the MCMC samples as

$$M_K^{i,n} = \tan(\phi_1^n) \cdot \log(P^{i,n}) + \tan(\phi_2^n) \cdot [\text{Fe}/\text{H}]^{i,n} + b^n, \quad (15)$$

where the superindex i tags stars (from 1 to N) and the superindex n tags the sample in the MCMC set of samples. In the right hand panel we show the same diagram, but computing the absolute magnitude from the measured apparent magnitude and the MCMC parallax:

$$M_K^{i,n} = \hat{m}_0^i + 5 \cdot \log(\varpi^{i,n}) - 10, \quad (16)$$

where \hat{m}_0^i represents the measured value of the apparent magnitude corrected for the measured extinction (that is, we only

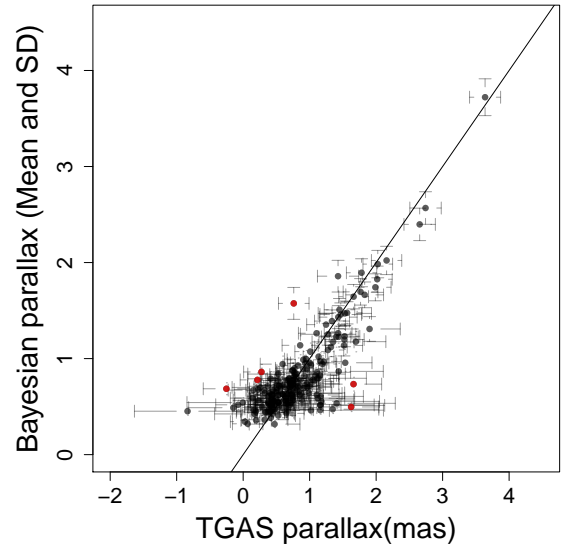


Fig. 9: Comparison between the TGAS parallaxes and the maximum a posteriori estimates from the hierarchical model (HM). The error bars correspond to the TGAS parallax uncertainties (horizontal) and the standard deviations of the posterior sample distributions (vertical). The red circles correspond to stars with parallax difference beyond 2 times the combined uncertainties.

use the parallaxes from the model, but the extinction and apparent magnitudes used in Eq. 16 are those measured and listed in Paper I). The black circles correspond to the discrepant sources marked by red circles in Fig. 9. The outlier at $\log(P) \approx -0.26$ corresponds to V363 Cas. This star was classified as a double-mode pulsator by Hajdu et al. (2009). A detailed analysis of its nature is beyond the scope of this paper, but we note that it would be consistent with its discrepant position in the diagrams. These two panels can be compared to the period-absolute magnitude diagram drawn using only the bare measurements of parallax, apparent magnitude, extinction and period (Fig. 11). The absolute magnitude is computed using the maximum likelihood estimate of the distance (the reciprocal of the parallax). It is important to remark that Fig. 11 is limitedness in three respects: first, stars with negative parallaxes are omitted from the plot for obvious reasons; second, the vertical error bars are very poor approximations because they were computed using the linear approximation to error propagation $\sigma_{M_K} = 2.17 \cdot \sigma_{\varpi} / \varpi$. This is obviously wrong for many of the stars in the sample with large fractional errors of the parallax and asymmetric uncertainties of the absolute magnitudes. Finally, the maximum likelihood estimates have a number of caveats as discussed by Astraatmadja & Bailer-Jones (2017). Note the very different scales in Figs. 10 and 11.

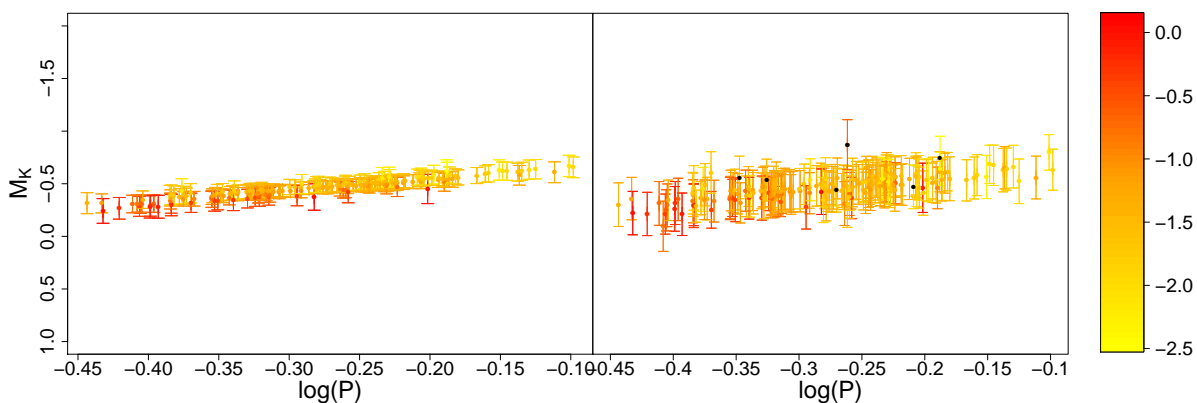


Fig. 10: *Left*. Samples of the PLZ relations derived from the MCMC samples for $[Fe/H] = -1.46$ (the mode of the distribution of metallicity measurements $[Fe/H]_i$ (grey lines)) and period- M_K values inferred by the HM and computed according to Eq. 15. *Right*. As in the left panel, but with M_K computed according to Eq. 16. The colour encodes the metallicity according to the scale on the right.

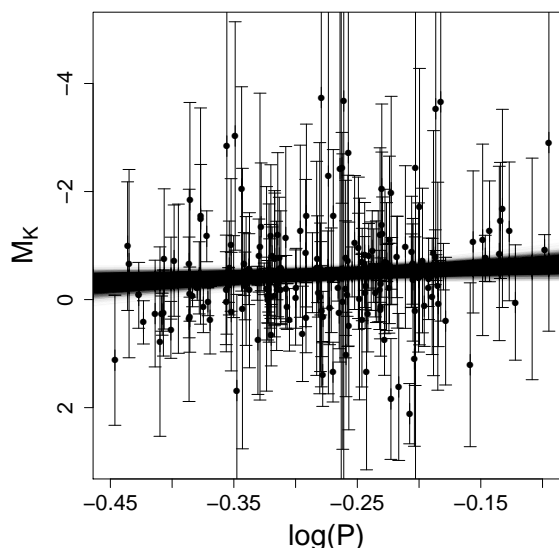


Fig. 11: PLZ relations defined by the MCMC samples for the value of $[Fe/H] = -1.46$ (dark grey lines) and the measured periods and absolute magnitudes inferred by using the reciprocal of the parallax as (maximum likelihood) estimate of the distance. The error bars correspond to the (flawed) approximation of the confidence intervals.

5. The parallax priors

As mentioned above, we used a log-skew-normal prior for the parallaxes of RR Lyrae stars. Fig. 12 shows the MCMC posterior samples of the hyperparameters of this prior (location β , scale γ and shape α) obtained by our HM when it is trained with the RR Lyrae sample used in Paper I and Fig. 13 shows a histogram of measured parallaxes (black bars) and several samples of the prior. It is important to remark that there is not a single prior for the parallaxes. On the contrary, we define the prior simply as a distribution (the skew-log-normal) the parameters of which are inferred as part of the hierarchical model. Therefore, we obtain

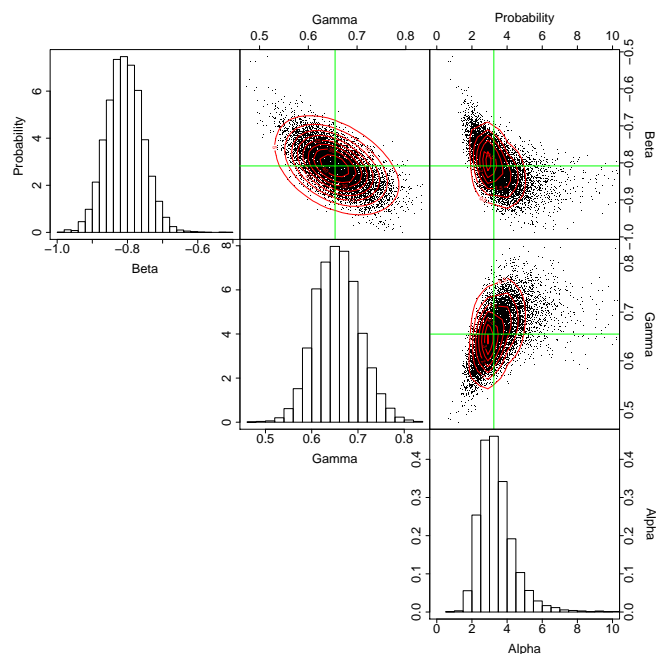


Fig. 12: Marginal posterior distributions from the MCMC samples of the location, shape and scale hyperparameters of the log-skew-normal prior.

as result a posterior probability distribution for the prior parameters. Hence, what we draw in Fig. 13 as continuous blue lines are priors drawn from the posterior distributions of the prior parameters. Obviously, the priors have zero probability density for negative values of the parallax and have an extended tail towards large values of the parallax.

As part of our study and in light of the particular RR Lyrae data set analysed in this paper we have investigated what could be a suitable functional form for the parallax prior. For that purpose we have used the semi-synthetic sample of true parallaxes that was described in Section 3. We have fitted three candidate

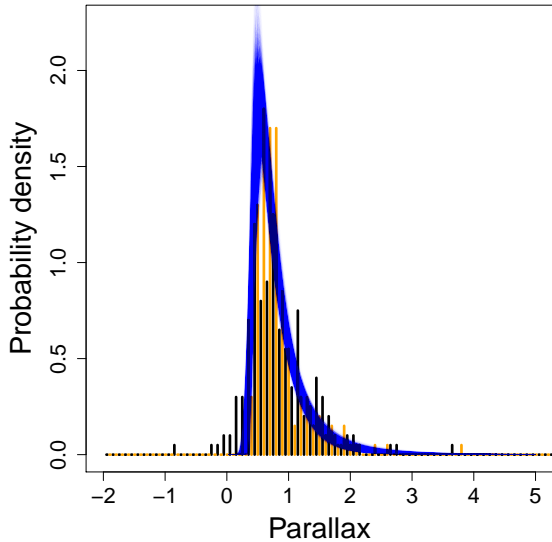


Fig. 13: Histograms of the TGAS (black) and HM (orange) parallaxes. The blue lines are prior probabilities defined by HM MCMC samples of β , γ and α (the log-skew-normal parameters).

prior distributions to this sample using the maximum likelihood estimate: the log-skew-normal prior used in this paper, the log-normal prior used in Paper I and the EDVD prior of Bailer-Jones (2015)

$$p(\varpi) = \frac{1}{2L^3\varpi^4} \exp\left(-\frac{1}{\varpi L}\right). \quad (17)$$

Fig. 14 shows the results of these fittings. By looking at the EDVD prior curve of the Figure (depicted in red) one sees that it assigns a higher probability density to lower parallaxes (higher distances) than the LSN and LN priors. It shows also that the probability density function (PDF) of the fitted EDVD prior is wider and its maximum is shifted to lower parallaxes with respect to the other two PDFs. As a consequence the fitted EDVD prior also assigns less probability density to intermediate parallaxes (those which are around 0.7 mas). Hence, given that we demonstrated in Sec. 3 that an over and underestimation of true parallaxes in the lower and upper bounds of the distribution of measured parallaxes causes an underestimation of the PLZ $\log(P)$ slope presence of a $\log(P)$ -parallax correlation, the use of an EDVD prior for parallaxes in our HM should improve the estimation of this slope. To check this hypothesis we have validated our HM again but using an EDVD prior. We have taken for the EDVD scale length hyperparameter L an exponential hyperprior with inverse scale factor equal to 0.5 kpc. Fig. 15 compares the inferred parallaxes to the true parallaxes of the semi-synthetic data sets A and B. We see that in simulation B (bottom panel), when compared to Fig. 6 of Sec. 3, the overestimation and underestimation of the inferred parallaxes is now less severe. Hence, the EDVD prior results in inferences that are significantly less affected by the existing correlation between periods and parallaxes. In fact, the inferred $\log(P)$ slopes for simulation B were, for the HM with SLN and EDVD prior, respectively of -0.87 and -1.18 mag/dex. We have also analysed the effect of the correlation between true parallaxes and periods on the inferred true

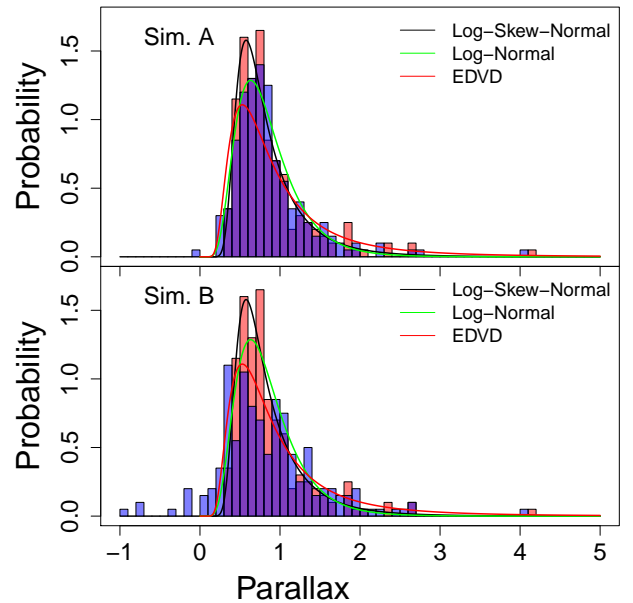


Fig. 14: Histograms of true and observed parallaxes of the simulations A and B described in Sec. 3. The true parallaxes (represented in orange colour) are common to both simulations. The solid lines correspond to three alternative prior probability density functions fitted to the true parallaxes: log-skew-normal (black line), log-normal (green line) and EDVD (red line).

parallaxes. For that, we have constructed a third semi-synthetic data set C in which we have simulated the true parallaxes from an EDVD prior distribution that has been fitted to the true parallaxes of datasets A and B. Hence, true periods and true parallaxes of data set C are uncorrelated by construction. In this case, as in the data set B, we have generated the observed parallaxes by using the TGAS parallax uncertainties. Figure 16 illustrates that true parallaxes are better recovered by the HM model with the log-skew-normal prior when true parallaxes and periods are uncorrelated. The posterior medians obtained for the $\log(P)$ slope and for the intercept were ≈ -1.75 mag/dex (assuming a period in days) and ≈ -0.72 mag for this latter simulation, which are closer to the literature values. To end this Section we summarize the results of the Bayesian analysis performed on the RR Lyrae sample of Paper I when an EDVD prior is adopted for our HM and compare them with the results obtained for the LSN and SN prior distributions. Figure 17 shows the posterior samples for the PLZ parameters in selected 2D projections when an EDVD prior is used in our HM and Table 2 compares the posterior medians and credible intervals of the PLZ relationship parameters for the three prior distributions for parallaxes tested in this article. We observe a clear increase (in absolute value) of the posterior median of the $\log(P)$ slope ($\tan(\phi_1) \approx -1.13$ mag/dex), for the EDVD with regard to its posterior medians inferred by using the other two priors (≈ -0.85 and ≈ -0.84 mag/dex for the LN and SLN prior). This results are consistent with the results of validating the HM with the data set B summarized in this Section above.

Prior	$\tan(\phi_1)$	$\tan(\phi_2)$	b	w
Log-Skew-Normal	$-0.85^{+0.57}_{-0.69}$	$+0.08^{+0.13}_{-0.13}$	$-0.60^{+0.29}_{-0.32}$	$0.18^{+0.08}_{-0.07}$
EDVD	$-1.13^{+0.74}_{-0.86}$	$+0.12^{+0.14}_{-0.14}$	$-0.63^{+0.38}_{-0.32}$	$0.13^{+0.05}_{-0.07}$
Log-Normal	$-0.84^{+0.67}_{-0.71}$	$+0.07^{+0.11}_{-0.11}$	$-0.59^{+0.29}_{-0.31}$	$0.13^{+0.06}_{-0.06}$

Table 2: Summary statistics of the posterior samples of the *PLZ* relationship parameters corresponding to the three prior distributions tested in this article. The posterior distribution of each parameter is summarized by the median plus minus the difference in absolute value between the median and the 90th and 10th percentiles.

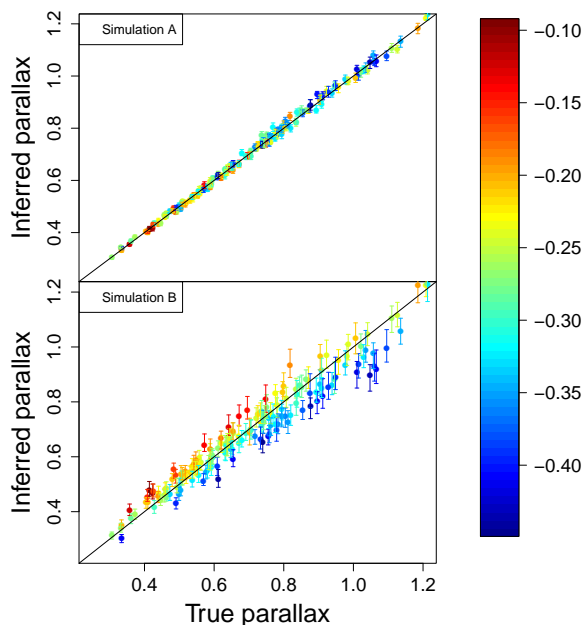


Fig. 15: Comparison between inferred and true parallaxes for validation sets A and B when a HM with an EDVD prior is used. The colour encodes the value of the decadic logarithm of the period in days according to the colour scale on the right.

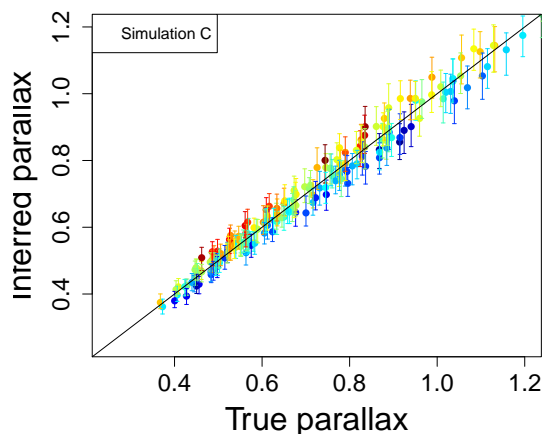


Fig. 16: Comparison between inferred and true parallaxes for validation set C when a HM with an EDVD prior is used. Colour encoding is the same as in Fig. 15.

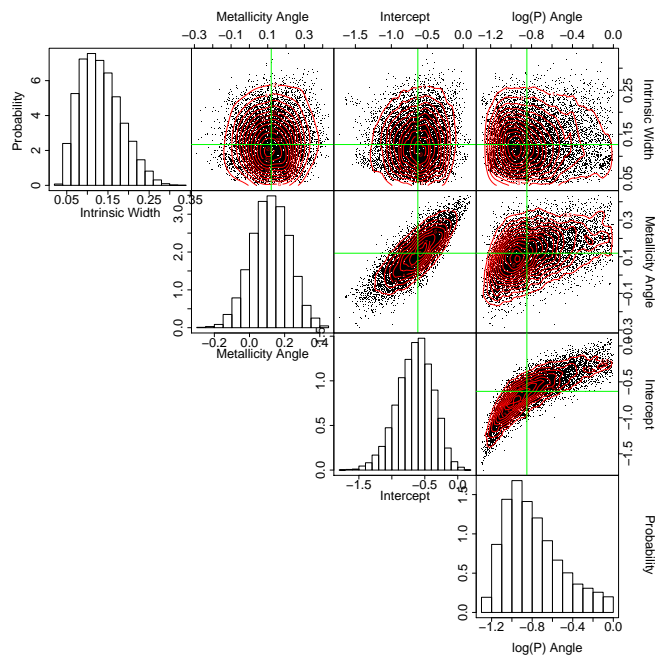


Fig. 17: Marginal posterior distributions from the MCMC samples for the HM with an EDVD prior for parallaxes. The diagonal shows the uni-dimensional marginal distributions for the intrinsic width of the relationship, the angle of the metallicity term in the linear relation, the intercept and the angle of the $\log(P)$ term.

6. Sensitivity analysis

In this Section we analyse the sensitivity of our HM when the prior distribution of true parallaxes is modelled by an EDVD. In the Bayesian statistical framework a sensitivity analysis consists of studying the influence of the prior distribution assigned to some critical parameters in the model on the posterior samples of each parameter of interests. Given that most of the prior distributions in our model were chosen to be non-informative, we do not expect significant variations of the posterior distributions for other choices of their prior parameters. Changing the prior definition for $\log(P)$ or $[\text{Fe}/\text{H}]$ has absolutely no impact in the posterior inferences unless we use very informative narrow priors. We have tried different priors for the scale parameter L of the intrinsic width w prior distribution from 0.1 to 10 kpc.

Table 3 compares the posterior medians and credible intervals of the *PLZ* relationship parameters for the different prior choices. In all cases, we have fixed the inverse scale of the hyperprior of L (the scale length parameter of the exponential decay in the EDVD prior) to a value of 0.5 kpc. Larger values of the inverse scale extend the support of the prior to smaller val-

ues of the parallax but without significant effects in the resulting posteriors.

Parameter	$\tan(\phi_1)$	$\tan(\phi_2)$	b	w
$\pi(w) = \text{Exp}(0.1)$	$-1.27^{+0.74}_{-0.78}$	$+0.12^{+0.13}_{-0.14}$	$-0.69^{+0.34}_{-0.35}$	$+0.13^{+0.07}_{-0.06}$
$\pi(w) = \text{Exp}(1)$	$-1.13^{+0.74}_{-0.86}$	$+0.12^{+0.14}_{-0.14}$	$-0.63^{+0.38}_{-0.32}$	$+0.13^{+0.05}_{-0.07}$
$\pi(w) = \text{Exp}(10)$	$-1.31^{+0.72}_{-0.70}$	$+0.10^{+0.15}_{-0.11}$	$-0.71^{+0.33}_{-0.28}$	$+0.11^{+0.07}_{-0.06}$
$\pi(w) = \text{Exp}(50)$	$-1.33^{+0.77}_{-0.72}$	$+0.11^{+0.14}_{-0.14}$	$-0.72^{+0.34}_{-0.33}$	$+0.03^{+0.03}_{-0.01}$
$\pi(\phi_1) = \text{U}(-3.14/2, +3.14/2)$	$-1.15^{+0.77}_{-0.80}$	$+0.13^{+0.14}_{-0.14}$	$-0.64^{+0.35}_{-0.35}$	$+0.14^{+0.07}_{-0.05}$
$\pi(\phi_2) = \text{U}(-3.14/2, +3.14/2)$	$-1.27^{+0.78}_{-0.95}$	$+0.11^{+0.14}_{-0.14}$	$-0.69^{+0.34}_{-0.38}$	$+0.12^{+0.07}_{-0.07}$

Table 3: Summary statistics corresponding to the sensitivity analysis performed to the HM when an EDVD prior is used for parallaxes.

7. Summary and conclusions

In this paper we have applied the hierarchical Bayesian methodology to infer estimators for the parameters of the *PLZ* relationship in the *K*-band for fundamental and first overtone RR Lyrae stars. We have extended the analysis performed in Paper I by testing new prior distributions and analysing correlations in the data, their influence on the inference and the consequences of the prior choice.

In Sec. 3 we have demonstrated through the use of semi-synthetic data that the RR Lyrae sample used in Paper I presents strong correlations that result in different spatial distributions for the different metallicities and periods. As a result, the larger parallax uncertainties are not spread uniformly in period but concentrated in the region of long periods, thus making the inference results strongly dependent on the prior. For small parallax uncertainties (typically one order of magnitude smaller than the TGAS uncertainties) the effect of parallax uncertainties on the parameters of the *PLZ* relation inferred by our HM is minimal. In such simulated scenario our HM is able to successfully recover one of the *PLZ* relation of Muraveva et al. (2015) as expected. On the contrary, for the TGAS parallax uncertainties used in Paper I we experience a drastic degradation in the performance of the HM and a severe underestimation of the $\log(P)$ slope term of the *PLZ* relation.

In Sec. 4 we have applied our HM to the sample of 200 fundamental and first overtone RR Lyrae stars and Gaia DR1 parallaxes used in Paper I. Our HM has inferred MCMC posterior samples corresponding to parameters of the *PLZ* relation that are far away from the values reported in the literature. The slope of the $\log(P)$ term has been severely underestimated by the HM and the zero-point has been systematically overestimated. We conclude that these anomalous results are caused by a negative correlation between the periods and parallaxes of the RR Lyrae sample.

In Sec. 5 we have demonstrated that a suitable prior functional form may improve the Bayesian inference of the coefficients of the *PLZ* relationship in an scenario of large parallax uncertainties. This prior should have the property of supporting well the lowest (close to zero) and highest true parallaxes, because it is crucial that the absolute magnitudes be correctly inferred for the tails of the parallax distribution in order to avoid the underestimation of the *PLZ* $\log(P)$ slope.

Both scenarios of large and small parallax uncertainties and the problem of the sample representativeness certainly offer us the opportunity to explore new lines of research. In a scenario of small parallax uncertainties one could evaluate the possibility of using even more flexible prior distributions than the SLN prior, for example a Gaussian mixture (GM). We have evaluated (although not reported here) the use of a GM prior for parallaxes but it clearly underperforms the EDVD or the SLN prior. In

a scenario with large parallax uncertainties and a sample with strong correlations such as the one used in Paper I we recommend the exploration of metallicity dependent priors, which will anyhow be less necessary with the improved parallax uncertainties of subsequent *Gaia* data releases.

References

- Astraatmadja, T. L. & Bailer-Jones, C. 2017, in American Astronomical Society Meeting Abstracts, Vol. 229, American Astronomical Society Meeting Abstracts, 134.06
- Azzalini, A. 1985, *Scandinavian Journal of Statistics*, 12, 171
- Bailer-Jones, C. A. L. 2015, *Publications of the Astronomical Society of the Pacific*, 127, 994
- Carpenter, B., Gelman, A., Hoffman, M., et al. 2017, *Journal of Statistical Software*, 76, 1
- Gaia Collaboration, Clementini, G., Eyer, L., et al. 2017, *A&A*, 605, A79
- Gelman, A., Carlin, J. B., Stern, H. S., & Rubin, D. B. 2004, *Bayesian Data Analysis* (Chapman & Hall/CRC)
- Gelman, A. & Hill, J. 2007, *Data analysis using regression and multi-level/hierarchical models*, Vol. Analytical methods for social research (New York: Cambridge University Press), xxii, 625 p
- Hajdu, G., Jurcsik, J., & Sodor, A. 2009, *Information Bulletin on Variable Stars*, 5882
- Hoffman, M. D. & Gelman, A. 2014, *J. Mach. Learn. Res.*, 15, 1593
- Lauritzen, S. 1996, *Graphical Models* (Oxford University Press)
- Lindgren, L., Lammers, U., Bastian, U., et al. 2016, *A&A*, 595, A4
- Luri, X., Brown, A. G. A., Sarro, L. M., et al. 2018, *A&A*, submitted
- Muraveva, T., Palmer, M., Clementini, G., et al. 2015, *The Astrophysical Journal*, 807, 127
- Pearl, J. 1988, *Probabilistic Reasoning in Intelligent Systems: Networks of Plausible Inference* (Morgan Kaufmann Pub)
- Robert, C. & Casella, G. 2013, *Monte Carlo Statistical Methods*, Springer Texts in Statistics (Springer New York)
- Sesar, B., Fouesneau, M., Price-Whelan, A. M., et al. 2017, *The Astrophysical Journal*, 838, 107
- Wright, E. L., Eisenhardt, P. R. M., Mainzer, A. K., et al. 2010, *AJ*, 140, 1868